E-Article

Depth of the Biomass Maximum Affects the Rules of Resource Competition in a Water Column

Alexei B. Ryabov* and Bernd Blasius

Institute for Chemistry and Biology of the Marine Environment (ICBM), Carl von Ossietzky University of Oldenburg, Carl-von-Ossietzky-Straße 9-11, 26111 Oldenburg, Germany

Submitted August 12, 2013; Accepted April 21, 2014; Electronically published October 6, 2014

Online enhancement: appendix.

ABSTRACT: The theory of resource competition in spatially extended systems with resources and biomass fluxes is far from trivial. Here, we analyze the competition between two phytoplankton species for light and a nutrient in a weakly mixed water column. We develop a general framework for such an analysis and show that the competition outcome can be largely understood from a single parameter, the slope of the invasion threshold in the plane of resources. Using this approach, we show that the competition outcome crucially depends on the depth of the biomass maximum. Under eutrophic conditions, when the phytoplankton production peaks on the surface, species composition depends on the ratio of resource supplies, and the competition outcome follows the "classic" rule: coexistence is possible if each competitor has the greatest effect on its most limiting resource. By contrast, in oligotrophic systems, characterized by deep biomass maxima, the absolute level of resource supplies drives species composition, and coexistence becomes more feasible if each competitor mostly consumes its least limiting resource. Finally, when the production peaks in the subsurface, good nutrient competitors are favored. Our findings are supported by empirical data.

Keywords: biodiversity, coexistence, resource competition, invasion analysis, invasion thresholds, meta-ecosystem, phytoplankton, metacommunities, deep chlorophyll maximum.

Introduction

The composition of phytoplankton—a major constituent of marine and freshwater ecosystems (Falkowski 2012)—is hard to predict (Fox et al. 2010). Although phytoplankton communities are notable for their enormous diversity (Hutchinson 1961), they are typically dominated by a few species or functional groups that can differ significantly between water bodies and successive years in the same location (Vigil et al. 2009). A mechanistic explanation of these varying patterns of phytoplankton dominance in terms of underlying processes remains a major challenge for ecological theory.

One of the main factors shaping the structure of phytoplankton communities is the competition for limiting resources, such as light and nutrients. The classic theory of resource competition revolves around the so-called R^* rule, which states that a consumer with the lowest requirement of a resource will exclude all other species in competition for this resource (MacArthur 1972; León and Tumpson 1975; Tilman 1980, 1982; Chase and Leibold 2003). The R^* rule describes community composition in homogeneous systems. Its extension for spatially heterogeneous environments is not trivial (Grover 1997; Chesson 2000), mainly because its basic assumptions are violated in the presence of resource and biomass flows (Leibold et al. 2004; Gravel et al. 2010; Morozov 2010) but also because the distributions of resources and phytoplankton cells are interrelated through consumption and growth processes, so that resource heterogeneity can emerge dynamically from biotic interactions (Ryabov et al. 2010).

These complexities can be resolved in the two limiting cases of either neglecting the effect of diffusion on the spatial distribution of species (Huston and DeAngelis 1994; Yoshiyama et al. 2009) or assuming an infinite mixing rate (Huisman and Weissing 1995; Diehl 2002; Yoshiyama et al. 2009). These limits, however, fail to describe most natural systems, which are characterized by moderate levels of mixing. So far, such systems could be studied only numerically (Huisman et al. 1999; Troost et al. 2005; Dutkiewicz et al. 2009).

Recently, we developed a graphical approach to analyze resource competition in a moderately mixed water column where the intensity of light decreases and the nutrient concentration increases with depth (Ryabov and Blasius 2011). In such a system, with opposing gradients of two essential resources, the classic R^* rule is inapplicable because a competitor with high requirements of one resource can benefit from a low dependence on the other by ad-

* Corresponding author; e-mail: alexey.ryabov@uni-oldenburg.de.

Am. Nat. 2014. Vol. 184, pp. E132–E146.
0003-0147/2014/18405-54893$15.00.
DOI: 10.1086/677544

justing its vertical position. To extend the R^* rule for systems with spatial resource gradients, we introduced the notion of an invasion threshold, defined as the maximal resource requirements for a consumer to invade in the presence of a resident (Ryabov and Blasius 2011). Applying this notion, we were able to predict the competition outcome in the deep layers of a water column. In this case, coexistence requires that each species has the least influence on the resource that mostly limits its own growth—a rule that is diametrically opposed to the coexistence criterion in a uniform system (Tilman 1980, 1982).

While this approach describes two-species competition in a spatially heterogeneous system, it is applicable only far from the system boundaries. In particular, it did not include the influence of the surface of the water column on the net growth rates and biomass distributions, and therefore we could address only the competition outcome in the deep layers (Ryabov and Blasius 2011). As yet, no satisfying theoretical framework exists for describing species competition in the whole water column.

In this article, we study the competition between two phytoplankton species for light and a nutrient in a weakly mixed water column. We complement numerical simulations with a graphical approach for invasion analysis and show that the competition outcome can be largely understood from a single parameter, the slope of the invasion threshold in the plane of resources. Thereby, we develop a theory of resource competition that is valid for the whole water column.

To develop such a theory, we identify two distinct boundary effects when the bulk of the biomass approaches the surface. First, biomass losses from turbulent mixing are reduced, increasing the fitness of the competitors (Cantrell and Cosner 1998; Ryabov and Blasius 2008). Second, the possibility of spatial segregation of the two competitors is suppressed, which increases interspecific competition and effectively reduces fitness. These two antagonistic effects greatly complicate the dynamics of resource competition in a water column, because different depths favor coexistence of distinct groups of species.

To resolve these issues, we study the competition outcome in dependence on the depth of the biomass maximum. We find that a pair of competitors that can coexist in the surface layer most likely will not coexist in the deep layers, and vice versa. In this way we not only identify generic routes of phytoplankton dominance shifts with change of the vertical position in the water column but are also able to reconcile the rules of species coexistence in the deep layers (Ryabov and Blasius 2011) with the classic rules in a uniform system (Tilman 1980, 1982).

This transition from one set of rules to the other occurs in the subsurface layer. We show that this layer also obtains a special role as a niche for good nutrient competitors. In contrast, the surface phytoplankton layer is favorable for superior light competitors, while in the deep layers the competition outcome is driven by the magnitudes of the resource supplies rather than their ratio: increasing either incident light intensity or the nutrient supply favors good light competitors.

All these effects increase the environmentally mediated variability of phytoplankton composition and give rise to intricate patterns of competitive outcomes and transitions. In spite of their complexity, we show that these patterns can be understood and predicted with a simple diagram technique. The complex model outcomes are highly relevant to field data. By comparing our model results with data on phytoplankton distributions in Lake Tanganyika, we show that our theory can explain the vertical variations in the chlorophytes-cyanobacteria assemblage of this system. Our theoretical findings demonstrate that in deep aquatic basins the composition of phytoplankton can depend nonmonotonically on the depth of the production layer and on other parameters. This might lead to divergent consequences in different regions of the ocean in the case of water pollution or global warming.

Methods

Model

To model resource competition of phytoplankton in a water column, we use a system of reaction-diffusion equations (Radach and Maier-Reimer 1975; Shigesada and Okubo 1981; Klausmeier and Litchman 2001; Huisman et al. 2006). Let $P_i(z, t)$ denote the density of phytoplankton species i ($i = 1, 2$) at depth z and time t. Its dynamics can be described as

$$\frac{\partial P_i}{\partial t} = \mu_i(N, I)P_i - mP_i + D\frac{\partial^2 P_i}{\partial z^2}, \tag{1}$$

where $\mu_i(N, I)$ is the growth rate, which depends on the local light intensity $I(z, t)$ and nutrient concentration $N(z, t)$, m is the mortality rate, and D is the turbulent diffusivity. Assuming that phytoplankton cannot diffuse across the surface and bottom of the water column, we complement equation (1) by the zero-flux boundary condition

$$\left.\frac{\partial P_i(z, t)}{\partial z}\right|_{z=0, Z_B} = 0,$$

where Z_B is the water column depth. The dependence of the growth rate on resources is approximated by Liebig's law of the minimum, where the limitation of growth follows Monod kinetics,

$$\mu_i(N, I) = \mu_{\max} \min\left(\frac{N}{H_{N,i} + N}, \frac{I}{H_{I,i} + I}\right), \quad (2)$$

with the maximal growth rate $\mu_{\max}$ and the half-saturation constants $H_{N,i}$ and $H_{I,i}$. The nutrient distribution is shaped by the consumption and diffusion processes, modeled as

$$\frac{\partial N}{\partial t} = -\sum_{i=1}^{2} \alpha_i \mu_i(N, I) P_i + D\frac{\partial^2 N}{\partial z^2}, \quad (3)$$

where α_i is the amount of the nutrient that is consumed to produce a new cell of species *i*. As the boundary conditions, we assume zero flux of nutrients across the surface and a constant nutrient level at the bottom,

$$\left.\frac{\partial N(z, t)}{\partial z}\right|_{z=0} = 0,$$
$$N(Z_B) = N_B.$$

These boundary conditions assume that all nutrient input enters from the bottom of the water column, which is typical for macronutrients, such as phosphorus or nitrogen, that are recycled in the deep layers or in the sediment (Moore et al. 2013). Finally, the incident light is absorbed by water and phytoplankton cells,

$$I(z) = I_{in} \exp\left(-K_{bg} z - \int_0^z \sum_{i=1}^{2} k_i P_i(\xi, t) d\xi\right) \quad (4)$$

(Kirk 1994), where I_{in} is the incident light intensity, K_{bg} is the water turbidity, and k_i is the light-attenuation coefficient of phytoplankton cells. The simulation details are found in appendix A and tables A1 and A2.

Invasion Analysis

Invasion analysis revolves around the ability or inability of each species to grow when rare and to invade a system dominated by its competitor. This framework is readily applied to the competition for two essential resources in a well-mixed system (Tilman 1980). The competitive ability of a species is represented in the resource plane by its zero–net growth isoclines (ZNGIs)—lines that divide the resource plane into areas of positive and negative population net growth (fig. 1*a*). Assuming equation (2) for the growth rate, we can calculate the critical values,

$$N_i^* = H_{N,i}\frac{m}{\mu_{\max} - m},$$
$$I_i^* = H_{I,i}\frac{m}{\mu_{\max} - m}, \quad (5)$$

and the ZNGIs take the form of two orthogonal lines (dashed lines in fig. 1*a*).

A growing population of the resident (species 1) will deplete resources, shifting the system state from the resource supply point *S* in the direction of the consumption vector CV_1, until the system state hits the population's ZNGI at the equilibrium point $E_1 = (\tilde{N}_1, \tilde{I}_1)$. The invasion of species 2 under these conditions is possible only if its resource requirements are less than E_1, that is, if they are located in the rectangular area where $I_2^* < \tilde{I}_1$ and $N_2^* < \tilde{N}_1$. This condition defines the invasion threshold IT_1 of species 1 in a well-mixed system (black line in fig. 1*a*).

Calculating the IT for each competitor as a resident allows us to infer the competition outcome. Consider, for example, the competition of species 1 and 2 from table A2 (see fig. 1*b*). In this example, species 1 is the better nutrient competitor ($H_{N,1} < H_{N,2}$) and species 2 is the better light competitor ($H_{I,2} < H_{I,1}$); however, species 2 reduces light less, relative to the nutrient consumption, than species 1 ($k_2 < k_1$), so that CV_2 has a shallower slope than CV_1. Under these conditions, the critical resource values of each species are located below the IT of its competitor. Thus, each of the two species can invade a system dominated by the other, and the two species will coexist. In general, coexistence in a uniform system is possible only if the species have a trade-off in resource requirements and each species has a relatively greater impact on its most limiting resource; otherwise, the outcome of competition can be bistable (Tilman 1980).

To extend this approach to a heterogeneous system, we define the invasion threshold (IT) of a resident species as the maximal resource requirements for a successful invader (Ryabov and Blasius 2011). The IT can be represented by a curve in the resource space. All species with critical resources N^* and I^* below this curve have a positive growth rate in the presence of the resident and can invade the spatial system. An exemplary IT of resident species 1 in a weakly mixed water column is shown by the black curve in figure 1*c*. The negative slope of the IT indicates a trade-off between invaders with low light requirements and those with low nutrient requirements. In this example, species 2 (blue), with higher nutrient and lower light requirements, can invade at a greater depth.

In the following, we assume that the competitors differ only in their half-saturation constants but are otherwise equal (i.e., the parameters μ_{max}, m, and D are identical for both species). In this case, the IT passes through the critical resources of the resident, which essentially simplifies the further analysis. The generalization to differences in μ_{max} and m is discussed in "Model Limitations and Conclusions."

The advantage of using the IT is that it allows us to perform an invasion analysis in a heterogeneous system, such as a weakly mixed water column, despite its inherent

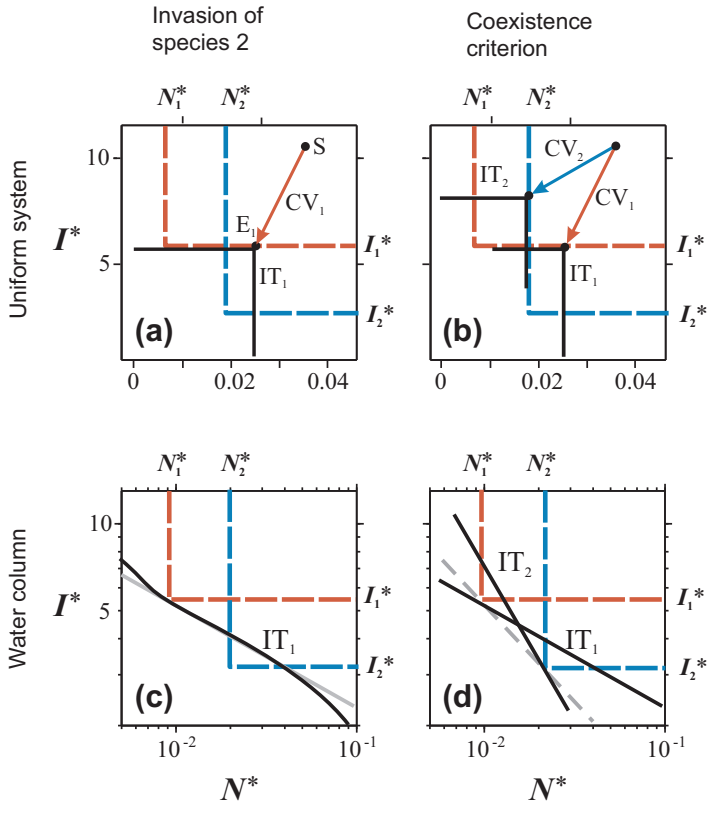

Figure 1: Invasion analysis in a uniform system (*top*) and an incompletely mixed water column (*bottom*). *a*, In the presence of resident species 1 (red), the equilibrium resource level E_1 is determined by the intersection of the consumption vector CV_1, starting at the resource supply point S, with the zero–net growth isocline (red dashed line; see text). The resource requirements of a successful invader (species 2, blue dashed line) should be located below the invasion threshold IT_1 (black line). *b*, Condition for coexistence: the critical resource values of each species are located below the invasion threshold in the presence of its competitor. *c*, In a weakly mixed water column, the invasion threshold IT_1 is represented by a curve (black line), which can be approximated by a straight line (gray line) with slope γ_i in the log-log plot; see equation (B1), available online. *d*, Same as *b*, but for a water column. The dashed gray line shows the critical slope, γ^*, of the ITs (eq. [6]).

complexities. Simple knowledge of the location and shape of the IT for each species suffices to infer the competition outcome. Ryabov and Blasius (2011) showed that the IT can be approximated by a straight line on a double-logarithmic scale (gray line in fig. 1*c*) if phytoplankton growth peaks in the deep layers of a water column. The invasion success then depends only on a single parameter, the slope γ_i of the resident's IT (see "Numerical Calculation of the IT and Its Slope γ" in app. B, available online, for further calculation details and "Logarithmic Resource Gradients" in app. B for an ecological interpretation of γ_i). A low value of γ_i is beneficial for low-light-adapted invaders, while a high γ_i value favors low-nutrient-adapted invaders (see IT_1 and IT_2, respectively, in fig. 1*d*). In this sense, the slope of the IT defines the "niche range" for possible invaders.

The critical value γ^* for the slope of the IT corresponds to the slope of a line passing through the critical resources of the two competitors (dashed gray line in fig. 1*d*). Assume, without loss of generality, that $N_2^* > N_1^*$ and $I_2^* < I_1^*$; then,

$$\gamma^* = -\frac{\ln I_2^*/I_1^*}{\ln N_2^*/N_1^*}. \tag{6}$$

Now we can formulate the following invasion criterion: a better nutrient competitor (e.g., species 1 in fig. 1*d*) can invade the system if its critical resource values yield a slope γ^* that is shallower than the slope of the residents' IT ($\gamma^* < \gamma_2$); in contrast, a better light competitor (e.g., species 2 in fig. 1*d*) can invade the system if its critical slope is steeper than the slope of the residents' IT ($\gamma^* > \gamma_1$). This gives rise to the following rules for the competition outcome: if $\gamma_1 < \gamma^* < \gamma_2$, the two species will coexist (see fig. 1*d*); if $\gamma_{1,2} > \gamma^*$, species 1 will dominate; if $\gamma_{1,2} < \gamma^*$, species 2 will dominate; finally, if $\gamma_1 > \gamma^* > \gamma_2$, neither of the species can invade, giving rise to alternative stable states (bistability).

Results

Location of the Production Layer

In general, the depth of the biomass maximum depends on many factors, such as resource supplies, species requirements, and environmental parameters (Klausmeier and Litchman 2001; Beckmann and Hense 2007). Here and below, we use the nutrient supply at the bottom of the water column, N_B, as our main control parameter to regulate the position of the biomass depth maximum.

Figure 2 shows typical equilibrium distributions of biomass (blue lines) and growth rates (black lines) obtained from numerical modeling of a single species. For all parameter values, positive net growth occurs in a relatively thin production layer (yellow areas). This positive net growth balances the losses of phytoplankton cells via diffusion into the unfavorable layers above and below the production layer. The emerging phytoplankton biomass in equilibrium results from the dynamic balance of the net growth and loss terms. However, as indicated in figure 2, the losses into the upper layers decrease as the production layer approaches the surface. This boundary effect enhances the fitness of consumers at a shallow depth, with drastic consequences on the competition outcome (see below).

We identify three characteristic phytoplankton profiles (fig. 2): deep chlorophyll maxima (DCM), subsurface layers (SSLs), and surface layers (SLs). These density profiles are also shown in figure 3 (*top*), together with the distributions of light (dashed gray line) and nutrient (black line). A DCM occurs for low levels of N_B. In this regime, the production layer is located far from the surface and the boundary effects are negligible; the population growth is limited simultaneously by both resources (by light below the production layer and by nutrients above; fig. 3*a*, 3*b*, *top*). With increasing N_B the production layer rises until, at a certain depth, the biomass distribution is affected by the boundary at the surface, yielding an SSL. The transition from a DCM to an SSL is gradual and can be detected differently. On the basis of numerical calculation, we call a biomass distribution an SSL if $P_i(0) \geq \max(P_i(z))/2$. In an SSL, both resources are still limiting (fig. 3*c*, *top*). Finally, an SL occurs, when only light limits biomass growth. In this regime, the production layer is directly constrained by the surface of the water column and the biomass attains a maximal value at the surface (fig. 3*d*, *top*).

Invasibility at Different Depths

We now investigate the influence of the depth of the production layer on invasibility. For this, we calculate the ITs formed by the resident population (here and below, the resident is species 2) for various values of the nutrient supply N_B (fig. 3, *bottom*). As shown, the slope of the IT changes with variation in N_B, giving rise to an effective

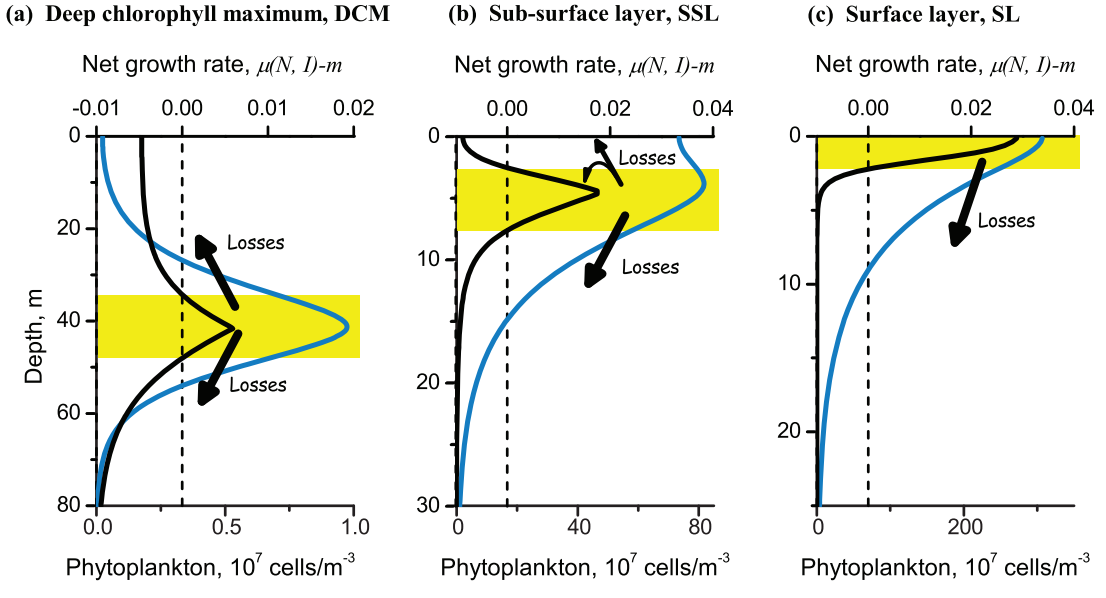

Figure 2: Phytoplankton distribution (blue lines) and biomass losses (arrows) in dependence of the location of the production layer in a single-species community. The production layer (yellow area) is a layer with positive net growth rate (black lines). Increasing the nutrient supply, N_B, (from left to right) moves the production layer to the top, passing from a deep chlorophyll maximum (DCM; *a*), through a subsurface layer (SSL; *b*), to a surface layer (SL; *c*). The closer to the surface the production layer is located, the less biomass is lost upward. Parameter values are listed in tables A1 and A2 (species 2); $N_B = 0.5$, 30, and 70 mmol nutrient m^{-3} in *a*, *b*, and *c*, respectively.

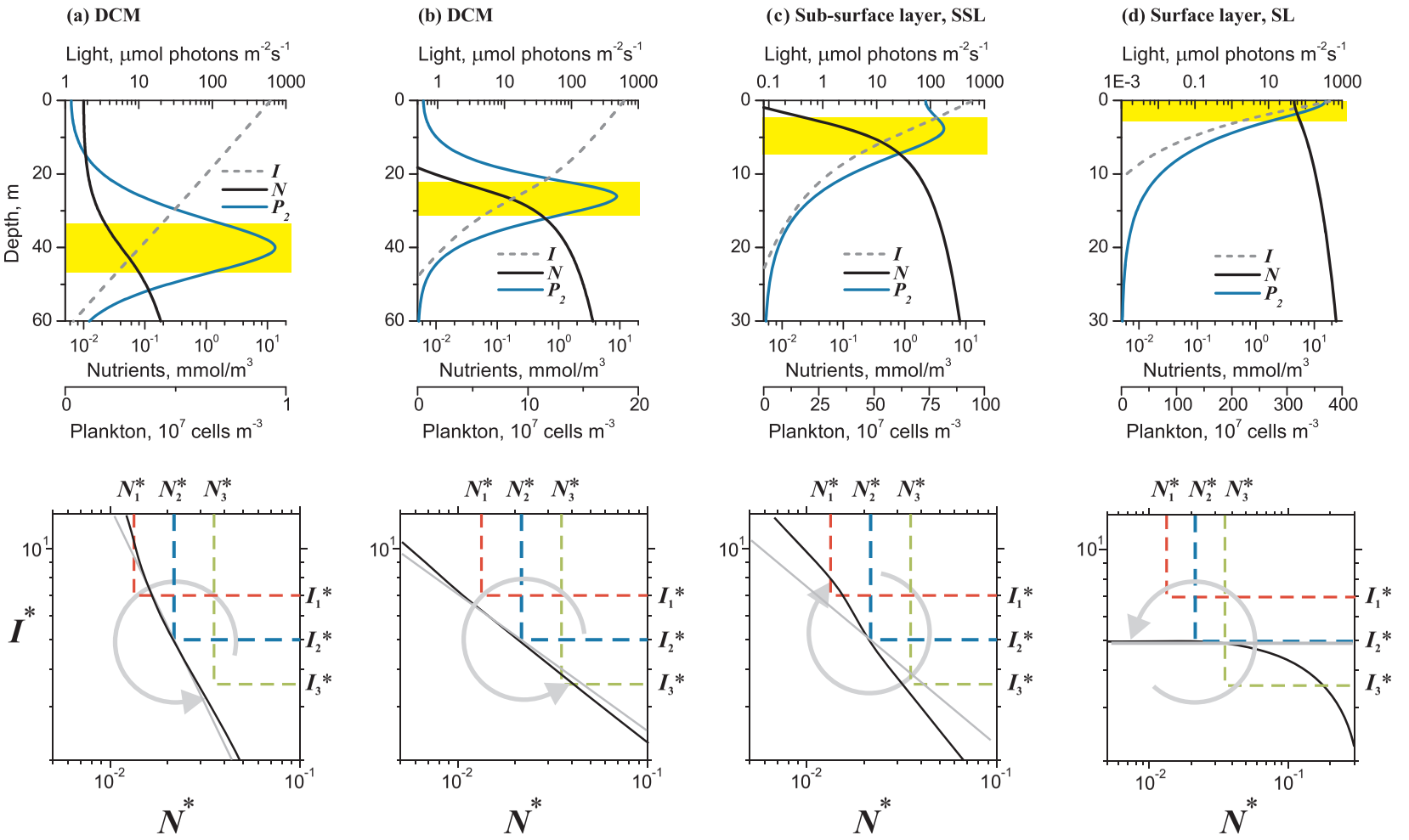

Figure 3: Invasion analysis for different phytoplankton configurations. *Top*, biomass distribution $P_2(z)$ of the resident species 2 (blue line), light intensity $I(z)$ (dashed line), and nutrient distribution $N(z)$ (black solid line) for different vertical positions of the production layer (yellow area). *Bottom*, the corresponding invasion conditions for a good nutrient competitor (species 1; red zero–net growth isocline [ZNGI]) and a good light competitor (species 3; green ZNGI) in the presence of resident species 2 (blue ZNGI). The invasion thresholds (ITs) and their slopes estimated by equation (B1), available online, are shown by black and gray lines, respectively. The direction of rotation of the ITs with increasing N_B is shown by gray arrows. The ITs are obtained from numerical calculations based on 2,000 simulated invasions by species with different H_N and H_I. The nutrient supply N_B, from left to right, equals 0.5, 8.0, 30, and 70 mmol nutrient m^{-3}.

rotation of the IT in distinct directions in the different depth regimes (indicated by the gray arrows). This allows us to identify the conditions under which a better nutrient competitor (species 1) or a better light competitor (species 3) can invade, as shown below.

Deep Chlorophyll Maximum (DCM). At low values of N_B, the biomass maximum of the resident species occurs in the deep layers (fig. 3*a*, 3*b*, *top*). Numerical and analytical calculations (Ryabov and Blasius 2011; Ryabov 2012) show that, in this range, increasing N_B typically leads to a counterclockwise rotation of the IT, which results in a shallower slope of the IT (black lines in fig. 3*a*, 3*b*, *bottom*). This manifests a transition from conditions favorable for invaders with low N^* to conditions favorable for invaders with low I^*. In other words, nutrient enrichment in the DCM regime enlarges the invasion niche of better light competitors (relative to the resident), and it reduces the invasion niche of better nutrient competitors.

In theory, increasing N_B may also have the opposite effect, giving rise to a steeper slope of the ITs (see "Logarithmic Resource Gradients" in app. B). This transition occurs in the extreme case when the light attenuation by phytoplankton exceeds the background turbidity. This, however, is rather atypical, because the DCM usually contributes less than half to the total light attenuation (Zielinski et al. 2002; Hamilton et al. 2010; Hylander et al. 2011).

Subsurface Layer (SSL). A further increase of N_B moves the production layer upward into the SSL (fig. 3*c*). This favors the survival of the consumer because the diffusive loss-flow of cells is reflected back into the production layer by the surface. The strength of this positive boundary effect is hard to analyze in a rigorous way (Cantrell and Cosner 1991). In general, the influence of the surface depends on the location of the production layer. It will be stronger for a low-nutrient-adapted invader, as it is characterized by a production peak at shallower depths, and weaker for a high-nutrient-adapted invader, as it is characterized by a deeper production maximum. Consequently, the survival conditions will be more favorable for superior nutrient competitors and less favorable for superior light competitors. As a result (compare the black and gray lines in fig. 3*c*, *bottom*), in the SSL the true slope of the IT is steeper than is predicted by theory (see eq. [B1], in "Logarithmic Resource Gradients" in app. B). Thus, an increase of N_B yields a clockwise rotation of the IT, which, in comparison to a DCM regime, increases the invasion success of a better nutrient competitor.

Surface Layer (SL). This situation changes drastically when a further increase of N_B moves the production layer from the subsurface layer (SSL) into an SL (fig. 3*d*) and light becomes the main limiting factor. Under pure light limitation, a new species can invade independently of its N^* value as soon as its I^* is lower than the resident's I^*. Therefore, the invasion threshold (IT) approaches a straight horizontal line. Note that in this regime, the full IT resembles that of a uniform system (fig. 1*a*).

In figure 4, we represent the slopes of the IT (see "Numerical Calculation of the IT and Its Slope γ" in app. B for calculation details) as functions of N_B, calculated for monocultures of species 1 and 2 under two different light conditions. For convenience, we quantify the slope as an angle, arctan γ, that takes values within the finite interval $[0, \pi/2]$ (arctan $\gamma = 0$ for a horizontal IT and arctan $\gamma = \pi/2$ for a vertical IT). The figure reveals that the response of γ to a change in the nutrient supply is different in the three depth regimes (see also fig. 3). As a consequence, the curve arctan $\gamma(N_B)$ follows a characteristic nonmonotonic shape: the slope of the IT decreases with N_B in the

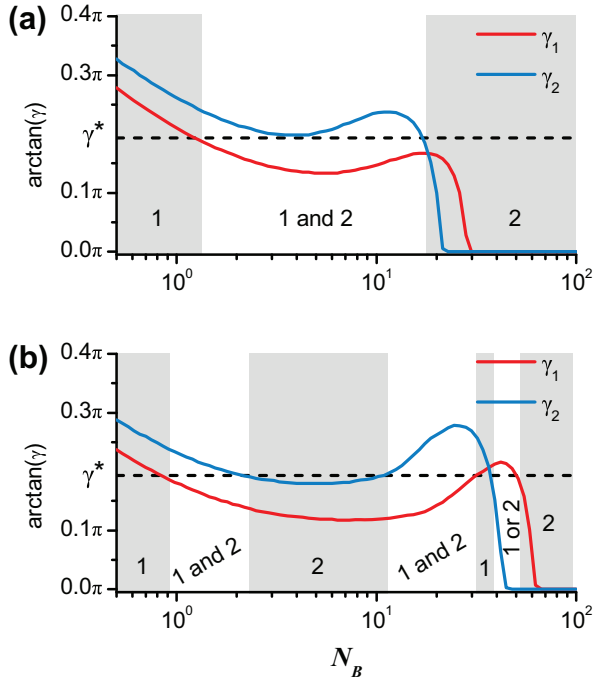

Figure 4: Possible transitions in species composition with increasing N_B; slopes γ_i of the invasion thresholds (ITs) in dependence of N_B for species 1 (a better nutrient competitor; red line) and species 2 (a better light competitor; blue line), obtained from numerical simulations and the resulting community composition (gray shading indicates dominance of a single species). For convenience, the slopes of ITs are expressed in radians as arctan γ. *a*, Each γ_i line has only one intersection with the critical level γ^* (dashed line). *b*, Multiple intersections of $\gamma_{1,2}(N_B)$ with the critical level γ^* lead to multiple transitions in the species composition. Parameter values: $I_{in} = 100$ (*a*) or 700 (*b*) μmol photons m^{-2} s^{-1}; the competitors have parameters of species 1 and 2′ (see table A2).

DCM regime (low values of N_B), it begins to rise and passes through a local maximum in the SSL regime (intermediate values of N_B), and finally it drops sharply to 0 in the SL regime (high values of N_B). These changes in the slope of the IT can be related to the variation of the niche size available for specific invaders: high values of γ favor invaders with low nutrient requirements, while low γ values are beneficial for low-light-adapted invaders.

Possible Transition in Species Composition

To find possible transitions in species composition, we calculate the slope of the IT in dependence of N_B for each competitor alone (see fig. 4). Then the crossings of the lines $\gamma_{1,2}(N_B)$ with γ^* will capture different invasion regimes. Note that the nutrient supply N_B affects the slope of the IT but not the critical resources and therefore also not the critical slope γ^* (eq. [6]). According to the invasion criterion (fig. 1*d*), the better nutrient competitor, species 1, can invade for all values of N_B for which the slope of the better light competitor (blue line in fig. 4) is above the critical line γ^* (dashed line). In contrast, species 2 can invade for all values of N_B for which the curve $\gamma_1(N_B)$ (red line) is below the critical line. Because of the nonmonotonic dependence, the line $\gamma_i(N_B)$ can cross the critical level γ^* more than once, which can give rise to a complex sequence of community assemblages.

A simple scenario occurs when every curve crosses the critical level only once (fig. 4*a*). Applying the invasibility criterion, we conclude that at the low end of this plot ($\gamma_{1,2} > \gamma^*$) species 1 wins, at the high end ($\gamma_{1,2} < \gamma^*$) species 2 wins, and in the intermediate range the two species coexist, because $\gamma_1 < \gamma^* < \gamma_2$. Species coexistence (as shown in fig. 4*a*) occurs when $\gamma_1(N_B)$ intersects the critical level at a lower N_B value than does $\gamma_2(N_B)$. In the reverse situation, if $\gamma_2(N_B)$ would first achieve the critical level, there would be an interval in which $\gamma_1 > \gamma^* > \gamma_2$, corresponding to alternative stable states. Thus, similar to uniform systems, we can observe either coexistence or bistability at intermediate values of resource availability.

The variability in the species composition can be much higher if the curves $\gamma_{1,2}(N_B)$ intersect the critical level more than once. For instance, in the scenario that is shown in figure 4*b*, we observe two ranges of coexistence, one range of bistability, and four ranges in which only one species dominates. This is only one of many potential transitions (see "Potential Transitions in Species Composition" in app. B and fig. B1; figs. B1–B7 available online). Despite the apparent complexity of these transitions, they can be understood qualitatively from the analysis of the IT slopes.

Competition Outcomes in the (N_B, I_{in}) Plane

To obtain a better insight into possible transitions between different community compositions, we now compare the competition outcomes in two differently parameterized groups of competitors, (species 1 and 2) and (species 1′ and 2′), reflecting different mechanisms of resource partitioning. Each group contains a better nutrient competitor (species 1 or 1′) and a better light competitor (species 2 or 2′), which are realized by adjusting the half-saturation constants H_I and H_N (see table A2). The two groups are distinguished by the effect of each competitor on its most limiting resource. This is realized by adjusting the light-attenuation coefficient of phytoplankton cells, k_p, for either the better nutrient or the better light competitor in each group (for simplicity, we change only the influence on the light intensity; we obtain similar results by changing the influence on the nutrients via variation of α_i). In the first group (species 1 and 2), each competitor has a relatively greater influence on its most limiting resource, $k_1 > k_2$. In the second group (species 1′ and 2′), each competitor has a relatively greater influence on its least limiting resource, $k_1' < k_2'$.

According to the resource-ratio theory (Tilman 1980), in a well-mixed system these two groups of competitors exhibit distinct patterns of competition outcomes. Besides the regions with dominance of a single species, the first group additionally admits a region of coexistence, and the second group additionally admits a region of bistability; however, it is not possible to find a pair of species that allows for all four competition outcomes.

By contrast, in a weakly mixed water column the situation is more complicated. Figures 5*a* and 5*b* show the outcome in the (N_B, I_{in}) parameter plane, revealing an intricate relationship between the species composition and the resource supplies. The overall patterns of competition outcomes correlate with the depth of the production maximum, z_{max}, defined by the condition $\mu(z_{max}) = \max \mu(z)$ (fig. B2). Low-light and high-nutrient conditions (bottom-right corner) lead to an SL, while high-light and low-nutrient conditions (top-left corner) lead to a DCM. In the SL good light competitors (species 2 or 2′) dominate, because they benefit from increasing N_B. Furthermore, when I_{in} is high enough (top-right corner), the species composition changes approximately with the ratio $\ln I_{in}/N_B$, as in a well-mixed water column (Huisman and Weissing 1995). In the DCM, low nutrient concentrations, in principle, should favor species 1 (or 1′). However, an increase in the light intensity leads to the dominance of species 2 (or 2′). Thus, in the DCM the species composition depends on the absolute levels of resource supplies, rather than their ratio.

In spite of the apparent similarity between figures 5*a* and 5*b*, there are also marked differences in the competition outcomes of the two groups of species. In the DCM and SSL regimes (the top-left part of the figures), the first

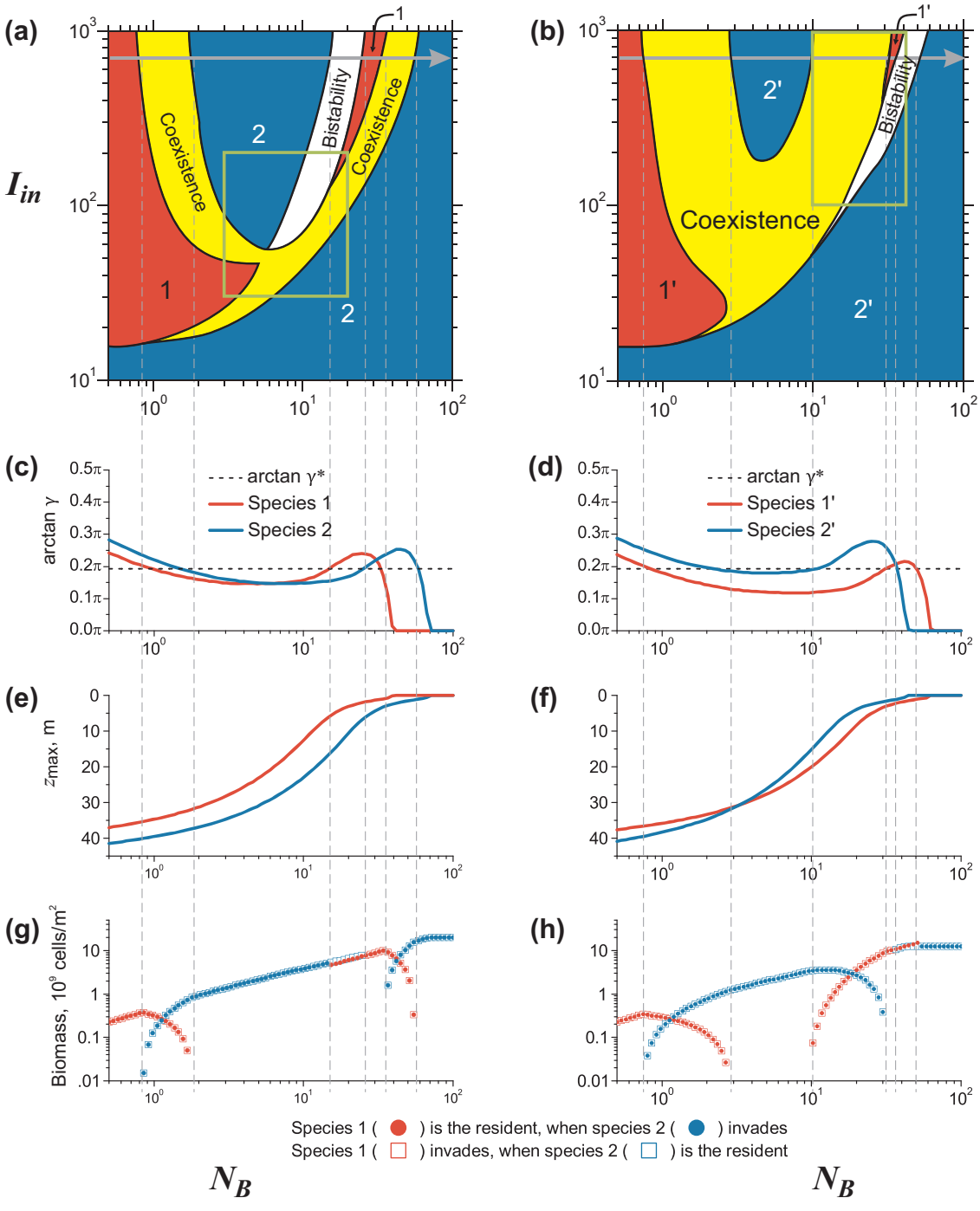

Figure 5: Competition between species parameterized to have a greater impact on their most limiting resource (*left*) or on their least limiting resource (*right*). *a*, *b*, Competition outcome in the (N_B, I_{in}) parameter plane. Different colors indicate different competition outcomes: dominance of species 1 or 1′ (red), dominance of species 2 or 2′ (blue), coexistence (yellow), and bistability (white). The green boxes indicate the resource ranges that are analyzed in more detail in figure B3. The gray arrows indicate the cross sections (I_{in} = 700 μmol photons m^{-2} s^{-1}) for the detailed analysis shown in the bottom panels. *c*–*f*, Slopes of the invasion thresholds, arctan γ (*c*, *d*) and depths of the production maximum z_{max} (*e*, *f*) as a function of N_B in the presence of each competitor alone. *g*, *h*, Biomass of each competitor in the two-species model. The open and filled symbols represent, respectively, the results obtained when species 1 invades in the presence of species 2 and vice versa.

group of species has small ranges of coexistence and bistability, whereas the second group exhibits one large range of coexistence. In contrast, in the SL regime, the first group exhibits a range of coexistence and the second group a range of bistability.

The lower panels in figure 5 provide a more detailed analysis along the gradient of N_B, indicated by the gray arrows in figure 5*a*, 5*b*. These panels show the effects of the different light-attenuation coefficients in the two groups of species on the conditions for coexistence in the deep layer and the SSL (low N_B) or in the SL (high N_B). As shown in figure 5*e*, 5*f*, the production layer rises monotonically with N_B, passing from a DCM through an SSL until it reaches the surface in the SL. Figures 5*c* and 5*d* show the corresponding change in the slope of the IT. Consider first the range of low N_B. In this range, species 1 and 2 have rather similar values of γ_1 and γ_2 (fig. 5*c*), and the condition for coexistence $\gamma_1 < \gamma^* < \gamma_2$ is fulfilled only in a small interval of N_B values. By contrast, in the second species group, the difference between the slopes of the ITs is much larger (fig. 5*d*), giving rise to two wide areas of coexistence in the deep layer and the SSL.

In the range of high N_B (corresponding to an SL), we observe the opposite relationship. In the first species group, the growth of the low-nutrient-adapted but light-shading species 1 becomes light limited at a lower value of N_B than does the growth of species 2. Thus, γ_1 drops to 0 in a range of N_B where γ_2 is still greater than γ^* (fig. 5*c*). This promotes coexistence in the SL. In contrast, in the second group species 2′ strongly attenuates light and γ_2' drops to 0 in a range where $\gamma_1' > \gamma^*$, resulting in a range of N_B where the competition outcome is bistable.

Finally, note that the areas of coexistence and bistability in the resource plane seem to have a common boundary. In the vicinity of this boundary, we observe a second kind of bistability between coexistence and single-species dominance (Ryabov and Blasius 2011). In these transitions, the invasibility criterion fails: only one species can always invade the system, but it is not able to exclude its competitor if it has established. Figure B3 represents a detailed analysis within the resource ranges shown by green boxes (fig. 5*a*, 5*b*).

In "Dependence on the Model Parameters" in appendix B, we explore the effect of the model parameters, such as species physiological rates and environmental conditions, on the IT slopes to determine the parameter combinations that potentially promote coexistence. As shown in figures B4 and B5, the influence of parameters can be highly nontrivial and may depend crucially on the biomass depth. For instance, increasing either the incident light intensity or the nutrient favors good nutrient competitors in the DCM (fig. B5*a*). Increasing background turbidity or turbulent diffusivity favors good light competitors in the SL, but it increases the niche for good nutrient competitors in the DCM or the SSL (fig. B5*c*, B5*d*). Finally, the SSL effect is most pronounced in a well-illuminated water column (high I_{in} or low K_{bg}).

Discussion

The Effect of the Production Layer Location

We found that the phytoplankton composition and the rules of resource competition explicitly depend on the depth of the biomass maximum. The surface layer is favorable for the superior light competitor, as its occurrence implies strong light limitation of phytoplankton growth and eutrophic conditions. By contrast, in the subsurface layer (mesotrophic conditions), the superior nutrient competitor might dominate, because it experiences smaller biomass losses than the superior light competitor. In the deep layers, the competition outcome is driven by the magnitudes of the resource supplies rather than by their ratio: increasing either incident light intensity or the nutrient supply favors the good light competitor, while decreasing them favors the superior nutrient competitor. These conclusions are confirmed by numerical simulations of the competition outcomes in a wide range of resource supplies (fig. 5*a*, 5*b*) and by a detailed invasion analysis ("Dependence on the Model Parameters" in app. B).

Comparison with Field Data

To compare our results with field observations, we turn to the field data obtained in 2002–2006 in the equatorial Lake Tanganyika, off Mpulungu (Descy et al. 2005, 2010). Our model settings correspond to the lake conditions during the so-called wet seasons (October–April), when the water column is stable (Descy et al. 2010) and dominated by two phytoplankton groups: cyanobacteria and chlorophytes (Hecky and Kling 1981). Under these conditions, cyanobacteria—good light competitors (Grover 1997)—were relatively more abundant when the biomass maximum occurred in the surface layer or as a DCM (shown by the red circles in fig. 6*a*). In contrast, chlorophytes—good nutrient competitors (Litchman et al. 2007)—dominated in the subsurface layer (see "Lake Tanganyika" in app. B for further details). This is also illustrated by the three exemplary field depth profiles that are shown in figure 6*b*–6*d*. The temperature profiles (dashed lines) in these plots indicate nearly constant mixing throughout the water column (i.e., the absence of an upper mixed layer), as implied by our model. To fit the lake dynamics with our model, we used the parameter set given in table A3 and assumed that the depth of the biomass maximum is driven by the nutrient supply. As shown in figure 6*a*, the unimodal shape in the distribution of experimental data points is matched well by our model predictions (solid lines).

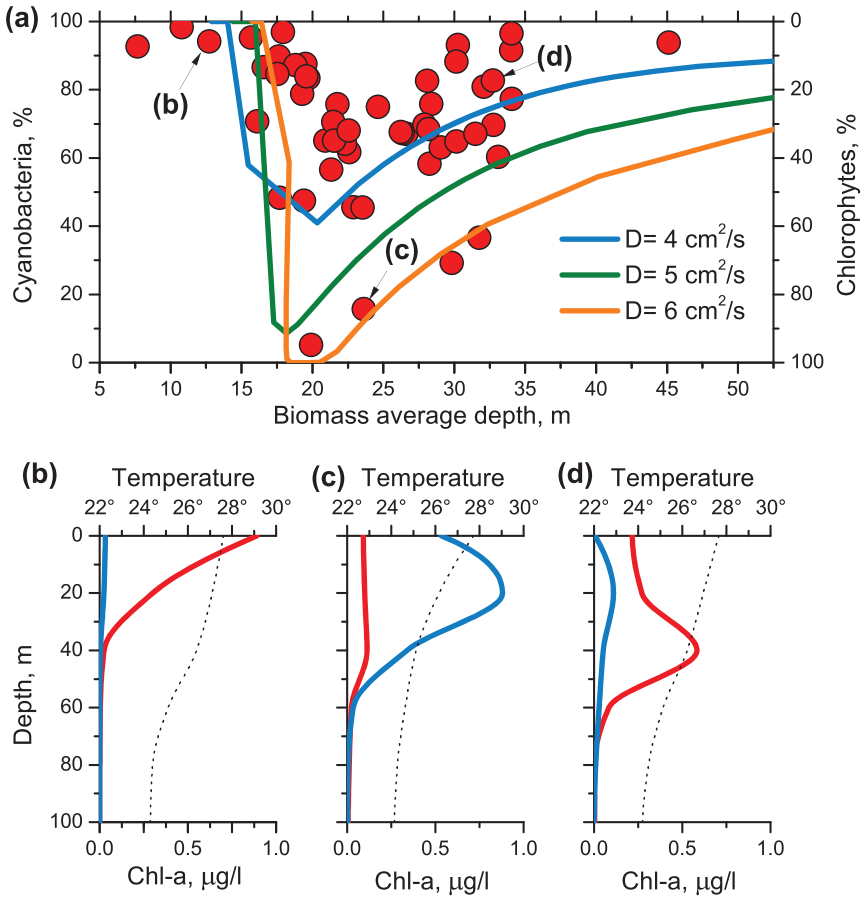

Figure 6: Comparison between field data (wet season, Lake Tanganyika, station Mpulungu) and the model outcomes. *a*, Species composition as a function of the average biomass depth. Cyanobacteria (red circles, left-hand scale) dominate when the bulk of the biomass (cyanobacteria + chlorophytes) is located either in the surface layer or in the deep layer, while chlorophytes (right-hand scale) are dominant in the subsurface layer at around 20 m depth (see "Lake Tanganyika" in app. B, available online, for details). Similar trends are obtained in our numerical simulations of the competition between two species with a resource trade-off. To fit the experimental data, we used the parameters presented in table A3. *b–d*, Exemplary experimental profiles of cyanobacteria (red lines), chlorophytes (blue lines), and temperature (dashed lines), corresponding to the points marked by the letters b–d in *a*. Chl-a = chlorophyll-*a*.

Our results are also close to the findings of Cermeño et al. (2008), who showed that in the Atlantic Ocean the coccolithophorid-to-diatom (C/D) ratio increases with the nutricline depth. The authors linked this effect to a trade-off between *r*-strategists (diatoms, who benefit from unstable conditions) and *K*-strategists (coccolithophorids, who win in stable environments). This explanation is plausible because smaller nutricline depths are typically attributed to unstable conditions in high latitudes. However, our results suggest that the same effect can also appear in stable environments and be linked to a trade-off in resource requirements. As coccolithophorids, relative to diatoms, require higher light intensity but lower nutrient concentrations in stable conditions (Aksnes et al. 1994; Iglesias-Rodríguez et al. 2002), they may be associated with our species 1 and diatoms with species 2. As shown in figure B7, with increasing N_B the production layer, and therefore the nutricline, moves toward the surface. While the production peaks in the deep layers, this induces a transition from species 1 to species 2, which corresponds a decrease in the C/D ratio with decreasing nutricline depth. In the subsurface layer, our model predicts an increase of species 1 abundance again. Surprisingly, figure 2 of Cermeño et al. (2008) also shows a local peak in the C/D ratio at approximately 30–40 m depth. Finally, in the surface layer, both the model and the experimental data show the dominance of species 2 (diatoms).

The Effect of Species Traits

The notion of resource consumption rates is crucial to resource-ratio theory (Tilman 1980). In a water column

this role belongs to the coefficients k and α, which define the effect of a growing population on the light and nutrient levels, respectively. We have shown that their effect on species coexistence crucially depends on the depth of the biomass maximum (fig. 5*a*, 5*b*). For coexistence in the surface layer, each competitor should mostly reduce its most limiting resource, which is essentially the same rule as for uniform systems (Tilman 1980). In contrast, in the interior layers coexistence is more likely if each competitor has a stronger effect on its least limiting resource (see also Ryabov and Blasius 2011).

To understand the reason for these different dynamic regimes, recall that in a uniform system coexistence relies on resource partitioning, so that each competitor becomes self-limited by its most required resource. Similarly, in the surface layer of a water column the growth of species 1, with high I^*, can become self-limited by light, because this species substantially attenuates light. This reduces the interspecific competition, and species 2, with low I^*, can invade. Note that a similar relationship was recently found for competition at the bottom of a water column between benthic and pelagic algae (Jäger and Diehl 2014). In the interior layers, however, the species growth is limited both by light below the production layer and by nutrients above it. For this reason, resource partitioning cannot reduce interspecific competition, and it is not surprising that another restriction can apply on the consumption rates. Now species 1 substantially attenuates light at greater depths—a niche of species 2, while species 1′, with low k_1', shapes a gentle light gradient, favoring the invasion of species 2′. In the subsurface layer, this effect is complimented by a correlation between the consumption rates and the location of production layer. As a result, in the subsurface layer, relative to the deep layers, we observe a stronger influence of the consumption rates on the possibility of coexistence or alternative stable states.

As another distinction from uniform systems, in a water column the potential of coexistence increases with the difference in species resource requirements, because a resident with low N^* shapes resource distributions in such a way that good light competitors obtain a large niche, and vice versa (fig. B4*c*, B4*d*). Thus, coexistence in a weakly mixed water column does not impose a strict relationship between the consumption rates.

Model Limitations and Conclusions

For the sake of simplicity, we assumed that the competitors do not sink and have the same m and μ_{max}. These assumptions were relaxed in Ryabov and Blasius (2011), where we considered competition in a DCM. In particular, it was shown that the species with the highest μ_{max} (*r*-strategists) should benefit in an environment with steep gradients of limiting resources. Extending this result to our present model, we suppose that an *r*-strategist can benefit from all factors leading to steep resource gradients, such as high K_{bg}, low D, or a high absolute level of resource supplies. This result is close to the findings of Huisman and Weissing (1995), who showed that in a well-mixed water column *r*-strategists win with an increasing absolute level of resource supplies.

Extending the analysis of phytoplankton competition in a water column, one can take into account seasonality (Litchman and Klausmeier 2001), interactions between three or more competitors or resources (Huisman and Weissing 2001; Dutkiewicz et al. 2009; Brauer et al. 2012), stochastic processes (Denaro et al. 2013), apparent competition (Leibold 1996), and other factors. Our proposed framework, based on invasion threshold (IT) analysis, can advantage this research for a number of reasons. First, the shape of an IT can clearly represent the system heterogeneity in relation to the invader's resource requirements (fig. 1). Second, this approach allows us to decompose a complex pattern of competition outcomes into simple and similar patterns for the slope of the IT (see fig. 4). Third, it compresses information, because it represents an interaction of one resident species with many potential invaders. Fourth, it provides a clear visual description of the trends in the invasibility conditions (fig. 3).

Finally, our approach provides new avenues for the data analysis of phytoplankton assemblages. In spite of clear relationships between phytoplankton traits (Litchman et al. 2007; Englund et al. 2011; Marañón et al. 2012), the phytoplankton dynamics often follows quite complex rules (Benincà et al. 2008). Our study reveals some aspects of this complexity. We show that even under stable conditions, the composition of phytoplankton depends nontrivially on the depth of the production layer, the resource levels, and often on the initial conditions. The understanding of such rules is crucial for disentangling the effect of different drivers in the analysis of field data (Gaedke and Schweizer 1993; Descy et al. 2010; Pomati et al. 2011) and also for projecting shifts in phytoplankton communities caused by nutrient pollution or climate change.

Acknowledgments

We thank J.-P. Descy and his group for providing us with data from subsequent projects on Lake Tanganyika funded by BELSPO (the Belgian Science Policy Office) in the framework of the program Science for Sustainable Development (SSD) and by FRS-FNRS (Fund for Scientific Research, Belgium). A.B.R. acknowledges support from the Helmholtz Virtual Institute (VH-VI-500, PolarTime).

APPENDIX A

Simulation

As initial conditions, we use a linear nutrient distribution changing from 0 at the surface to N_B at the bottom. The phytoplankton biomass initially has a uniform distribution of low density. For the numerical solution, the partial differential equations were discretized on a grid with a step size of 0.25 m. The resulting system of ordinary differential equations was solved by the CVODE package (http://www.netlib.org/ode) using the backward-differentiation method.

To perform the invasion analysis, the growth of the invader species is suppressed during the first 2,000 simulation days, to make sure that an equilibrium distribution of the resident species is established. Then the system is simulated for a duration of a further 50,000 (in some cases up to 200,000) days to obtain the final competition outcome. To test for bistability (alternative stable states), we perform a second simulation, in which the roles of invader and resident are exchanged. Such a long simulation time is necessary to localize the bifurcation lines (black lines in fig. 5*a*, 5*b*) separating different competition outcomes, because in the vicinity of a bifurcation the relaxation time exponentially increases. In a system subjected to strong seasonal changes, the outcome of competition in the vicinity of a bifurcation line should depend strongly on the succession order of the species.

Table A1: Model parameter values and their meaning

Symbol	Interpretation	Value	Units
Independent variables:			
t	Time		days
z	Depth		m
Dependent variables:			
$P(z, t)$	Population density		cells m^{-3}
$I(z, t)$	Light intensity		μmol photons m^{-2} s^{-1}
$N(z, t)$	Nutrient concentration		mmol nutrient m^{-3}
Parameters:			
I_{in}	Incident light intensity	1,000 (10–1,000)	μmol photons m^{-2} s^{-1}
K_{bg}	Background turbidity	.1	m^{-1}
Z_B	Depth of the water column	100	m
N_B	Nutrient concentration at Z_B	.5–100	mmol nutrient m^{-3}
D	Vertical turbulent diffusivity	.8	cm^2 s^{-1}
μ_{max}	Maximum specific growth rate	.04	h^{-1}
m	Specific loss rate	.01	h^{-1}

Table A2: Species parameters

Parameter	Units	Species 1	Species 2	Species 1′	Species 2′
Light shading		More	Less	More	Less
Good competitor for		Nutrient	Light	Nutrient	Light
H_I, half-saturation constant for light	μmol photons m^{-2} s^{-1}	21	15	21	15
I^*	μmol photons m^{-2} s^{-1}	7	5	7	5
H_N, half-saturation constant for nutrient	mmol nutrient m^{-3}	.04	.065	.04	.065
N^*	mmol nutrient m^{-3}	.0133	.0217	.0133	.0217
k, absorption coefficient of a cell	m^2 $cell^{-1}$	1.2×10^{-9}	$.75 \times 10^{-9}$	$.75 \times 10^{-9}$	1.2×10^{-9}
α, nutrient consumed per cell	mmol nutrient $cell^{-1}$	10^{-9}	10^{-9}	10^{-9}	10^{-9}

Table A3: Parameters used to fit Lake Tanganyika data in figure 6*a*

Symbol	Interpretation	Value	Units
Parameters:			
I_{in}	Incident light intensity	700	μmol photons m^{-2} s^{-1}
K_{bg}	Background turbidity	.04	m^{-1}
Z_B	Depth of the water column	100	m
N_B	Nutrient concentration at Z_B	.6–33	mmol nutrient m^{-3}
D	Vertical turbulent diffusivity	4, 5, 6	cm^2 s^{-1}
μ_{max}	Maximum specific growth rate	.025	h^{-1}
m	Specific loss rate	.01	h^{-1}
Species 1, chlorophytes:			
$H_{I,1}$	Half-saturation constant for light	30	μmol photons m^{-2} s^{-1}
$H_{N,1}$	Half-saturation constant for nutrient	.08	mmol nutrient m^{-3}
k_1	Absorption coefficient of a cell	$.4 \times 10^{-9}$	m^2 $cell^{-1}$
α_1	Nutrient consumed per cell	10^{-9}	mmol nutrient $cell^{-1}$
Species 2, cyanobacteria:			
$H_{I,2}$	Half-saturation constant for light	9	μmol photons m^{-2} s^{-1}
$H_{N,2}$	Half-saturation constant for nutrient	.19	mmol nutrient m^{-3}
k_2	Absorption coefficient of a cell	$.4 \times 10^{-9}$	m^2 $cell^{-1}$
α_2	Nutrient consumed per cell	10^{-9}	mmol nutrient cell

Note: The parameter values correspond to the conditions in Lake Tanganyika (Descy et al. 2010) and to the characteristics of freshwater phytoplankton (Agawin et al. 2007; Litchman et al. 2007; Schwaderer et al. 2011). We assumed a background turbidity of 0.04 m^{-1}, which is slightly lower than the minimal water turbidity observed in Lake Tanganyika (0.07 m^{-1}), to exclude the light attenuation by phytoplankton biomass.

Literature Cited

Agawin, N. S. R., S. Rabouille, M. J. W. Veldhuis, L. Servatius, S. Hol, H. M. J. van Overzee, and J. Huisman. 2007. Competition and facilitation between unicellular nitrogen-fixing cyanobacteria and non-nitrogen-fixing phytoplankton species. Limnology and Oceanography 52:2233–2248.

Aksnes, D. L., J. K. Egge, R. Rosland, and B. R. Heimdal. 1994. Representation of *Emiliania huxleyi* in phytoplankton simulation models. A first approach. Sarsia 79:291–300.

Beckmann, A., and I. Hense. 2007. Beneath the surface: characteristics of oceanic ecosystems under weak mixing conditions—a theoretical investigation. Progress in Oceanography 75:771–796.

Benincà, E., J. Huisman, R. Heerkloss, K. D. Jöhnk, P. Branco, E. H. van Nes, M. Scheffer, and S. P. Ellner. 2008. Chaos in a long-term experiment with a plankton community. Nature 451:822–825.

Brauer, V. S., M. Stomp, and J. Huisman. 2012. The nutrient-load hypothesis: patterns of resource limitation and community structure driven by competition for nutrients and light. American Naturalist 179:721–740.

Cantrell, R. S., and C. Cosner. 1991. The effects of spatial heterogeneity in population dynamics. Journal of Mathematical Biology 29:315–338.

———. 1998. On the effects of spatial heterogeneity on the persistence of interacting species. Journal of Mathematical Biology 37:103–145.

Cermeño, P., S. Dutkiewicz, R. P. Harris, M. Follows, O. Schofield, and P. G. Falkowski. 2008. The role of nutricline depth in regulating the ocean carbon cycle. Proceedings of the National Academy of Sciences of the USA 105:20344–20349.

Chase, J. M., and M. A. Leibold. 2003. Ecological niches: linking classical and contemporary approaches. University of Chicago Press, Chicago.

Chesson, P. 2000. Mechanisms of maintenance of species diversity. Annual Review of Ecology and Systematics 31:343–366.

Denaro, G., D. Valenti, B. Spagnolo, G. Basilone, S. Mazzola, S. W. Zgozi, S. Aronica, and A. Bonanno. 2013. Dynamics of two picophytoplankton groups in Mediterranean Sea: analysis of the deep chlorophyll maximum by a stochastic advection-reaction-diffusion model. PLoS ONE 8:e66765.

Descy, J. P., M. A. Hardy, S. Sténuite, S. Pirlot, B. Leporcq, I. Kimirei, B. Sekadende, S. R. Mwaitega, and D. Sinyenza. 2005. Phytoplankton pigments and community composition in Lake Tanganyika. Freshwater Biology 50:668–684.

Descy, J. P., A. L. Tarbe, S. Sténuite, S. Pirlot, J. Stimart, J. Vanderheyden, B. Leporcq, et al. 2010. Drivers of phytoplankton diversity in Lake Tanganyika. Hydrobiologia 653:29–44.

Diehl, S. 2002. Phytoplankton, light, and nutrients in a gradient of mixing depths: theory. Ecology 83:386–398.

Dutkiewicz, S., M. J. Follows, and J. G. Bragg. 2009. Modeling the coupling of ocean ecology and biogeochemistry. Global Biogeochemical Cycles 23:GB4017.

Englund, G., G. Öhlund, C. L. Hein, and S. Diehl. 2011. Temperature dependence of the functional response. Ecology Letters 14:914–921.

Falkowski, P. 2012. Ocean science: the power of plankton. Nature 483:S17–S20.

Fox, J. W., W. A. Nelson, and E. McCauley. 2010. Coexistence mechanisms and the paradox of the plankton: quantifying selection from noisy data. Ecology 91:1774–1786.

Gaedke, U., and A. Schweizer. 1993. The first decade of oligotrophication in Lake Constance. Oecologia (Berlin) 93:268–275.

Gravel, D., F. Guichard, M. Loreau, and N. Mouquet. 2010. Source and sink dynamics in meta-ecosystems. Ecology 91:2172–2184.

Grover, J. P. 1997. Resource competition. Chapman & Hall, London.

Hamilton, D. P., K. R. O'Brien, M. A. Burford, J. D. Brookes, and C. G. McBride. 2010. Vertical distributions of chlorophyll in deep, warm monomictic lakes. Aquatic Sciences 72:295–307.

Hecky, R. E., and H. J. Kling. 1981. The phytoplankton and protozooplankton of the euphotic zone of Lake Tanganyika: species composition, biomass, chlorophyll content, and spatio-temporal distribution. Limnology and Oceanography 26:548–564.

Huisman, J., N. N. Pham Thi, D. M. Karl, and B. Sommeijer. 2006. Reduced mixing generates oscillations and chaos in the oceanic deep chlorophyll maximum. Nature 439:322–325.

Huisman, J., P. van Oostveen, and F. J. Weissing. 1999. Species dynamics in phytoplankton blooms: incomplete mixing and competition for light. American Naturalist 154:46–68.

Huisman, J., and F. J. Weissing. 1995. Competition for nutrients and light in a mixed water column: a theoretical analysis. American Naturalist 146:536–564.

———. 2001. Fundamental unpredictability in multispecies competition. American Naturalist 157:488–494.

Huston, M. A., and D. L. DeAngelis. 1994. Competition and coexistence: the effects of resource transport and supply rates. American Naturalist 144:954–977.

Hutchinson, G. E. 1961. The paradox of the plankton. American Naturalist 95:137–145.

Hylander, S., T. Jephson, K. Lebret, J. Von Einem, T. Fagerberg, E. Balseiro, B. Modenutti, et al. 2011. Climate-induced input of turbid glacial meltwater affects vertical distribution and community composition of phyto-and zooplankton. Journal of Plankton Research 33:1239–1248.

Iglesias-Rodríguez, M. D., C. W. Brown, S. C. Doney, J. Kleypas, D. Kolber, Z. Kolber, P. K. Hayes, and P. G. Falkowski. 2002. Representing key phytoplankton functional groups in ocean carbon cycle models: coccolithophorids. Global Biogeochemical Cycles 16:47-1–47-20.

Jäger, C. G., and S. Diehl. 2014. Resource competition across habitat boundaries: asymmetric interactions between benthic and pelagic producers. Ecological Monographs 84:287–302.

Kirk, J. T. O. 1994. Light and photosynthesis in aquatic ecosystems. Cambridge University Press, Cambridge.

Klausmeier, C. A., and E. Litchman. 2001. Algal games: the vertical distribution of phytoplankton in poorly mixed water columns. Limnology and Oceanography 46:1998–2007.

Leibold, M. A. 1996. A graphical model of keystone predators in food webs: trophic regulation of abundance, incidence, and diversity patterns in communities. American Naturalist 147:784–812.

Leibold, M. A., M. Holyoak, N. Mouquet, P. Amarasekare, J. M. Chase, M. F. Hoopes, R. D. Holt, et al. 2004. The metacommunity concept: a framework for multi-scale community ecology. Ecology Letters 7: 601–613.

León, J. A., and D. B. Tumpson. 1975. Competition between two species for two complementary or substitutable resources. Journal of Theoretical Biology 50:185–201.

Litchman, E., and C. A. Klausmeier. 2001. Competition of phytoplankton under fluctuating light. American Naturalist 157:170–187.

Litchman, E., C. A. Klausmeier, O. M. Schofield, and P. G. Falkowski. 2007. The role of functional traits and trade-offs in structuring phytoplankton communities: scaling from cellular to ecosystem level. Ecology Letters 10:1170–1181.

MacArthur, R. H. 1972. Geographical ecology. Princeton University Press, Princeton, NJ.

Marañón, E., P. Cermeño, D. C. López-Sandoval, T. Rodríguez-Ramos, C. Sobrino, M. Huete-Ortega, J. M. Blanco, and J. Rodríguez. 2012. Unimodal size scaling of phytoplankton growth and the size dependence of nutrient uptake and use. Ecology Letters 16:371–379.

Moore, C. M., M. M. Mills, K. R. Arrigo, I. Berman-Frank, L. Bopp, P. W. Boyd, E. D. Galbraith, et al. 2013. Processes and patterns of oceanic nutrient limitation. Nature Geoscience 6:701–710.

Morozov, A. Y. 2010. Emergence of Holling type III zooplankton functional response: bringing together field evidence and mathematical modelling. Journal of Theoretical Biology 265:45–54.

Pomati, F., J. Jokela, M. Simona, M. Veronesi, and B. W. Ibelings. 2011. An automated platform for phytoplankton ecology and aquatic ecosystem monitoring. Environmental Science and Technology 45:9658–9665.

Radach G., and E. Maier-Reimer. 1975. The vertical structure of phytoplankton growth dynamics; a mathematical model. Mémoires de la Société Royale des Sciences de Liège 7:113–146.

Ryabov, A. 2012. Phytoplankton competition in deep biomass maximum. Theoretical Ecology 5:373–385.

Ryabov, A. B., and B. Blasius. 2008. Population growth and persistence in a heterogeneous environment: the role of diffusion and advection. Mathematical Modelling of Natural Phenomena 3(3):42–86.

———. 2011. A graphical theory of competition on spatial resource gradients. Ecology Letters 14:220–228.

Ryabov, A. B., L. Rudolf, and B. Blasius. 2010. Vertical distribution and composition of phytoplankton under the influence of an upper mixed layer. Journal of Theoretical Biology 263:120–133.

Schwaderer, A. S., K. Yoshiyama, P. de Tezanos Pinto, N. G. Swenson, C. A. Klausmeier, and E. Litchman. 2011. Eco-evolutionary differences in light utilization traits and distributions of freshwater phytoplankton. Limnology and Oceanography 56:589–598.

Shigesada, N., and A. Okubo. 1981. Analysis of the self-shading effect on algal vertical distribution in natural waters. Journal of Mathematical Biology 12:311–326.

Tilman, D. 1980. Resources: a graphical-mechanistic approach to competition and predation. American Naturalist 116:362–393.

———. 1982. Resource competition and community structure. Princeton University Press, Princeton, NJ.

Troost, T. A., B. W. Kooi, and S. Kooijman. 2005. Ecological specialization of mixotrophic plankton in a mixed water column. American Naturalist 166:E45–E61.

Vigil, P., P. D. Countway, J. Rose, D. J. Lonsdale, C. J. Gobler, and D. A. Caron. 2009. Rapid shifts in dominant taxa among microbial eukaryotes in estuarine ecosystems. Aquatic Microbial Ecology 54: 83–100.

Yoshiyama, K., J. P. Mellard, E. Litchman, and C. A. Klausmeier. 2009. Phytoplankton competition for nutrients and light in a stratified water column. American Naturalist 174:190–203.

Zielinski, O., O. Llinás, A. Oschlies, and R. Reuter. 2002. Underwater light field and its effect on a one-dimensional ecosystem model at station ESTOC, north of the Canary Islands. Deep-Sea Research Part II 49:3529–3542.

Associate Editor: Egbert H. van Nes
Editor: Troy Day